JOURNAL OF VIROLOGY, Aug. 2011, p. 7658–7671 Vol. 85, No. 15
0022-538X/11/$12.00 doi:10.1128/JVI.00473-11
Copyright © 2011, American Society for Microbiology. All Rights Reserved.

Clinical Outcome of Henipavirus Infection in Hamsters Is Determined by the Route and Dose of Infection▽

Barry Rockx,[1,3]* Douglas Brining,[2] Joshua Kramer,[4] Julie Callison,[1] Hideki Ebihara,[1] Keith Mansfield,[4] and Heinz Feldmann[1]

Laboratory of Virology,[1] Rocky Mountain Veterinary Branch,[2] Division of Intramural Research, National Institute of Allergy and Infectious Diseases, National Institutes of Health, Hamilton, Montana; Departments of Pathology and Microbiology & Immunology, University of Texas Medical Branch, Galveston, Texas[3]; and Harvard Medical School, Southborough, Massachusetts[4]

Received 8 March 2011/Accepted 10 May 2011

Nipah virus (NiV) and Hendra virus (HeV) are emerging zoonotic viruses and the causative agents of severe respiratory disease and encephalitis in humans. Little is known about the mechanisms that govern the development of respiratory and neurological disease. Using a hamster model of lethal NiV and HeV infection, we describe the role of the route and dose of infection on the clinical outcome and determine virus tropism and host responses following infection. Infection of hamster with a high dose of NiV or HeV resulted in acute respiratory distress. NiV initially replicated in the upper respiratory tract epithelium, whereas HeV initiated infection primarily in the interstitium. In contrast, infection with a low dose of NiV or HeV resulted in the development of neurological signs and more systemic spread of the virus through involvement of the endothelium. The development of neurological signs coincided with disruption of the blood-brain barrier (BBB) and expression of tumor necrosis alpha (TNF-α) and interleukin 1 β (IL-1β). In addition, interferon-inducible protein 10 (IP-10) was identified as playing an important role in NiV and HeV pathogenesis. These studies reveal novel information on the development and progression of NiV and HeV clinical disease, provide a mechanism for the differences in transmission observed between NiV and HeV outbreaks, and identify specific cytokines and chemokines that serve as important targets for treatment.

Hendra virus (HeV) and Nipah virus (NiV) are two members of the genus *Henipavirus* (family *Paramyxoviridae*) that cause severe respiratory illness and encephalitis in humans. HeV was the first member of the genus to be identified as the causative agent of an acute respiratory disease in horses in 1994 (30), and to date there have been 14 outbreaks in Australia, with at least one occurrence per year since 2006, most recently in May 2010. Only 7 human infections with HeV have been identified, of which 4 were fatal (57%) (25, 30, 36) (ProMed-Mail no. 20090903.3098). All patients initially presented with influenza-like illnesses (ILI) after an incubation period of 7 to 16 days. Lethal cases either developed pneumonitis and died from multiorgan failure or developed encephalitic manifestations (mild confusion and ataxia) and seizures.

The first cases of NiV were identified during an outbreak of severe febrile encephalitis in Malaysia and Singapore in 1998-1999 (9). A total of 276 patients with encephalitis were reported with 106 fatalities (38%). The primary mode of transmission to humans was believed to be pig to human, as this outbreak involved widespread respiratory disease in pigs and occupational exposure to pigs (1, 8). Since this outbreak, recurrent outbreaks of NiV in Bangladesh and India have involved more than 120 people (7, 16, 18). These outbreaks were associated with significantly higher case fatality rates, ranging from 67% to 92%. In addition, a higher prevalence of respiratory disease was observed during these outbreaks (18), and person-to-person contact with a patient carried a high risk of transmission (14, 15, 19).

Histopathological changes in the central nervous system (CNS) of fatal human HeV and NiV cases included systemic vasculitis and parenchymal necrosis, while in the lung, pathological findings included mainly vasculitis, fibrinoid necrosis, alveolar hemorrhage, pulmonary edema, and aspiration pneumonia (23, 36). Other organs that were affected included heart, kidney, and spleen and showed generally mild or focal inflammation. The development of syncytial multinucleated endothelial cells is characteristic for both HeV and NiV (36, 37). At present, the details on the pathogenesis and histopathological changes mediated by either HeV or NiV infection in humans is naturally derived from only the terminal stage of the disease. Therefore, in order to study pathogenesis over the time course of infection, a relevant animal disease model is needed that mimics the disease progression seen in humans.

Henipaviruses display a broad species tropism, and NiV has naturally infected several species of bats as well as pigs, humans, dogs, horses, and cats (34). Nonhuman primate models for both HeV and NiV and a ferret model for NiV have been described that mimic the clinical outcome observed with humans (4, 11, 29). Currently the only small-rodent disease model that mimics both HeV and NiV infection in humans is the Syrian golden hamster (13, 35). In this model both HeV and NiV infection via the intraperitoneal (i.p.) route caused primarily neurological disease; however, respiratory distress and sanguinous froth exuding from nares was observed in some HeV-infected animals. Interestingly, the majority of animals infected with NiV via the intranasal (i.n.) route developed

* Corresponding author. Mailing address: Departments of Pathology and Microbiology & Immunology, The University of Texas Medical Branch, 301 University Boulevard, Galveston, TX 77555-0610. Phone: (409) 266-6904. Fax: (409) 266-6810. E-mail: barry.rockx@utmb.edu.

▽ Published ahead of print on 18 May 2011.

neurological symptoms as well as labored breathing in the final stages of disease (35), while no information is available on i.n. infection of hamsters with HeV. The main histopathological findings included parenchymal infection in various organs, including the brain and lung, with vasculitis and multinucleated syncytial cells in the endothelium of many blood vessels (13, 35).

Limited information is available about the pathogenesis of HeV and NiV infection, and it is unknown what factors are involved in the development of either acute respiratory or neurological disease. We previously hypothesized that while a high dose of HeV resulted in the development of acute respiratory distress in the African green monkey model, a low dose would result in primarily neurological signs (29). Here we compare the pathogenesis of high- and low-dose infections of HeV and NiV in a lethal hamster model to more fully understand the impact of infection route and dose on the clinical outcome of disease. In addition, we characterize the host response following HeV and NiV infection.

MATERIALS AND METHODS

Ethics statement. Approval for animal experiments was obtained from the Rocky Mountain Laboratories (RML) Institutional Animal Care and Use Committee, Division of Intramural Research (DIR), National Institute of Allergy and Infectious Diseases (NIAID), National Institutes of Health (NIH). Animal work was performed by certified staff in an Association for Assessment and Accreditation of Laboratory Animal Care (AAALAC)-approved facility. Animal housing, care, and experimental protocols were in accordance with NIH guidelines.

Viruses and cells. HeV (GenBank no. AF017149) and NiV (Malaysia strain; GenBank no. AF212302) were kindly provided by the Special Pathogens Branch of the Centers for Disease Control and Prevention, Atlanta, GA. The viruses were propagated on Vero E6 cells in Dulbecco's minimal essential medium (DMEM) supplemented with 10% fetal calf serum (HyClone; Logan, UT), L-glutamine, penicillin, and streptomycin at 37°C in a humidified CO_2 incubator (5%). All infectious work was performed in a class II biological safety cabinet in a biosafety level 4 (BSL4) laboratory at the RML, DIR, NIAID, NIH.

Animal infection. Female Syrian golden hamsters (*Mesocricetus auratus*; 6-week-old HsdHan:AURA hamsters from Harlan Laboratories) were anesthetized by chamber induction (5 liters 100% O_2/min and 3 to 5% isoflurane). Each hamster was inoculated either intranasally (i.n.) with a 100-μl volume or intraperitoneally (i.p.) with a 200-μl volume of HeV, NiV, or phosphate-buffered saline (PBS). To determine the lethal dose at which 50% of the animals succumbed to infection (LD_{50}), groups of 5 animals were infected with 1, 10, 10^2, 10^3, 10^4, or 10^5 tissue culture doses leading to a 50% cytopathic effect (50% tissue culture infective dose [$TCID_{50}$]) of either HeV or NiV by i.n. or i.p. inoculation. The LD_{50} was calculated by the Reed-Muench method. To compare the pathogenesis levels of HeV and NiV infection, groups of 5 animals were infected with either 10^2 or 10^5 $TCID_{50}$ of HeV or NiV by i.n. inoculation. Animals were monitored daily for weight loss and clinical signs. For the pathogenesis study, groups of 5 animals were euthanized on various days postinfection (p.i.), and whole-blood samples (EDTA Vacutainer) as well as liver, spleen, kidney, bladder, trachea, left and right lung, heart, and brain (frontal, cerebellum, and stem) were removed for virus isolation, RNA extraction, and histological examination. Following necropsy, lungs were weighed as well as scored for the percentage of lesions.

To determine the permeability of the blood-brain barrier (BBB) during the induction of neurological disease by HeV and NiV infection, groups of 5 animals were challenged with 10^2 $TCID_{50}$ of HeV or NiV by i.n. inoculation. On days 5 (HeV) or 10 (NiV) p.i., animals were injected with 1 ml of a sterile 1% Evans blue (Sigma-Aldrich) solution in PBS by the i.p. route. Twenty-four hours after injection, animals were euthanized and transcardially perfused (60 ml PBS to remove access Evans blue in the blood), and brains removed.

Chest radiographs. A mobile digital radiography unit with a flat-panel digital detector (Sound Technologies Tru/Dr) and a portable X-ray generator (Poskom model PXP-HF) was used to acquire chest radiographs. The unit operates on veterinary-specific software system (VetPACS). Radiographic views acquired included ventrodorsal, right lateral, and left lateral thoracic images captured while the animals were under anesthesia.

Virus titrations. Tissue samples were weighed and homogenized in 10 equivalent volumes of DMEM to generate a 10% solution. The solution was centrifuged at 10,000 rpm under aerosol containment in a tabletop centrifuge for 5 min to pellet insoluble parts. Virus titration was performed using a $TCID_{50}$ assay on 96-well plates (1×10^4 Vero E6 cells per well) with 100 μl inoculum from 10-fold serial dilutions. Plates were incubated for 3 days at 37°C, and wells were scored for cytopathic effect (CPE). Virus concentrations were calculated as the $TCID_{50}$ per gram tissue.

RNA isolation and quantitative real-time PCR (RT-PCR) assays. Approximately 100 mg of tissue was stored in 1 ml RNAlater (Qiagen, Inc.) for 7 days at +4°C to stabilize RNA. RNAlater was completely removed, and tissues were homogenized and inactivated in 1 ml Trizol (Life Technologies) in a 2-ml cryovial using the Qiagen TissueLyser and stainless steel beads prior to removal from the BSL4 laboratory. Subsequently, RNA was isolated from tissues according to the manufacturer's instructions.

Host gene expression was determined as previously described (38). Briefly, the primers and probe that target the hamster interferon-inducible protein 10 (IP-10), gamma interferon (IFN-γ), tumor necrosis factor alpha (TNF-α), ribosomal protein L18 (RPL18), interleukin-1β (IL-1β), IL-4, IL-6, and IL-10 were used, and a one-step RT-PCR was done using Rotor-Gene Multiplex RT-PCR kits (Qiagen, Inc.). All RT-PCR mixtures contained 2 μl of RNA. Master mixes were set up according to the manufacturer's protocols. Each reaction was done in a total volume of 25 μl. Test samples were assayed using the Rotor Gene 6000 detection system (Qiagen, Inc.) with the following parameters: 50°C for 10 min, 95°C for 5 min, and 40 cycles of 95°C for 5 s, 60°C for 10 s. Threshold cycle (C_T) values representing hamster gene expression were analyzed with Rotor Gene 6000 software. The change for each gene was calculated using the mean of the change in C_T values (ΔC_T) normalized to the C_T values of RPL18 for each sample ($2^{-\Delta\Delta CT}$).

Histopathology and immunohistochemistry. All tissue samples were immersion fixed in 10% neutral buffered formalin for at least 7 days under BSL4 conditions. Prior to removal from the BSL4 laboratory, formalin was changed and specimens were processed under BSL2 conditions by conventional methods, embedded in paraffin, sectioned at a 5-μm thickness, and stained with hematoxylin and eosin (H&E). Tissues for immunohistochemistry were stained on the Discovery XT automated stainer (Ventana Medical Systems) using an anti-Nipah nucleoprotein antibody (1:5,000; kindly provided by C. Broder, Uniformed Services University, Bethesda, MD) and the DAB map detection kit (Ventana Medical Systems) (21). Nonimmune rabbit IgG was used as a negative staining control.

H&E-stained sections of lung, liver, spleen, kidney, bladder, brain, trachea, and skull (including nasal mucosa, olfactory cortex, cranial nerves, eyes, muscle, teeth, and bone in step sections) were examined for all animals by a pathologist. Pulmonary lesions were assigned a subjective score from + to +++ based on the severity of the lesions. In general, a score of + was given to those lungs with small, multifocal areas of peribronchial or random inflammation affecting <10% of the examined tissue. A score of ++ was given to those lungs with more severe inflammation, involving a larger percentage of lungs, 10 to 50%, but not yet entire lobes. A score of +++ was given to those lungs in which inflammation, edema, hemorrhage, and/or necrosis affected entire lung lobes or the majority of multiple lobes. A similar scoring system was used to assess the nasal mucosa and tracheal epithelium. For these tissues, scores of +, ++, and +++ represented mild, moderate, and severe histopathological changes, respectively. No scores were assessed for any other organs, and only the presence or absence of lesions was noted.

Immunohistochemistry using an anti-Nipah virus antibody was performed on lung, trachea, skull, and brain for a subset of cases, and these slides were examined by a pathologist. Lesions were assigned a score of + to +++ as described above for hematoxylin-and-eosin-stained sections.

RESULTS

Route and dose of infection determines clinical outcome. Syrian golden hamsters (*Mesocricetus auratus*) have previously been shown to be susceptible to infection with NiV and HeV (13, 35). In order to directly compare the virulence of HeV and NiV infection in this model, animals were inoculated with 10-fold dilutions (1 to 10^5 $TCID_{50}$) of HeV or NiV by the i.n. or i.p. route. The LD_{50} of animals by the i.n. and i.p. route was <1 and 6 $TCID_{50}$, respectively, and were identical for both

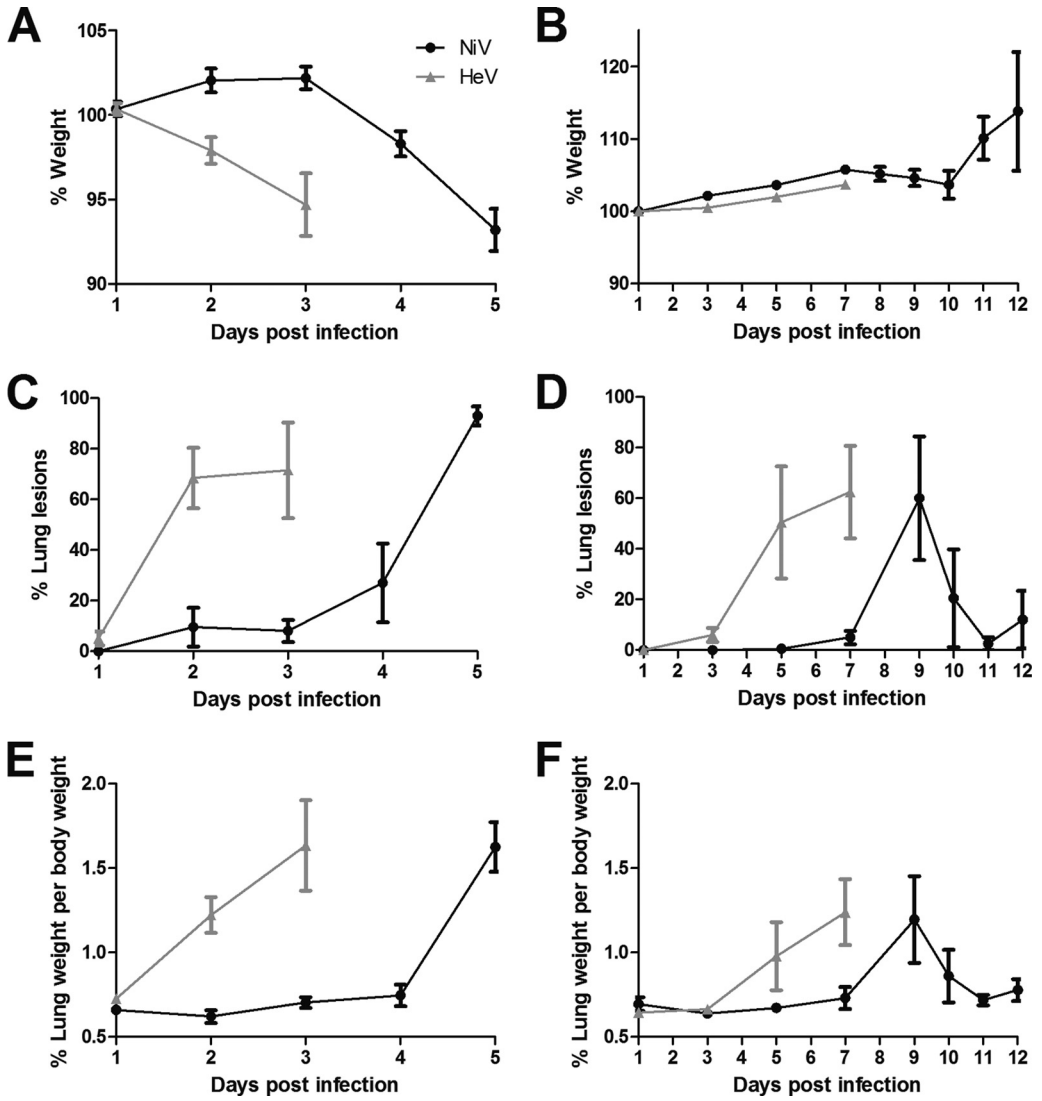

FIG. 1. The effect of infectious dose on the clinical outcome of HeV and NiV virus infection. Weight loss (A and B), percent lung lesions (C and D), and percent lung weight per body weight (E and F) results are shown for 6-week-old hamsters infected with a high (A, C, and E) or low (B, D, and F) dose of HeV (gray) and NiV (black). For panels A and B, body weights of infected hamsters were measured on a daily basis (n = 5 per group). Weight changes are expressed as the mean percent changes for infected animals relative to their weights at day zero. For panels C and D, gross pathological lung lesions are expressed as the mean percentage of the lung surface covered by lesions (n = 5 per group). For panels E and F, wet lung weights were measured for 5 animals per group each day and expressed as the percentage of lung weight per body weight. Error bars represent standard deviations.

NiV and HeV (data not shown). The average time to death of animals infected with 10^2 $TCID_{50}$ of virus via the i.n. route was significantly longer in NiV-infected animals (12 days) compared to HeV (7.5 days) (t test; $P < 0.05$). No significant differences in time to death were observed between NiV and HeV at a dose of 10^5 $TCID_{50}$ or following i.p. challenge. General signs included significant weight loss (>20%), reduced activity, and reluctance to move. Interestingly, animals infected with a high dose of NiV or HeV succumbed due to an acute onset of severe respiratory distress, whereas animals infected with a lower dose developed respiratory disease that progressed to neurological signs. Neurological signs included partial or complete paralysis, muscle fasciculations, and seizures. Respiratory signs included labored breathing and serosanguineous nasal and oral exudates.

Based on the differential clinical outcome due to the route and dose of infection, animals were challenged in subsequent experiments with either a high or low dose to induce a primarily respiratory or neurological disease, respectively.

Effect of NiV and HeV challenge doses. i.n. challenge of hamsters with a high dose (10^5 $TCID_{50}$) of HeV resulted in weight loss as early as day 2 p.i. (Fig. 1A). By day 3 p.i., all remaining HeV-infected animals were euthanized due to severe acute respiratory distress. Interestingly, animals infected with NiV showed a delay in weight loss and the development of respiratory signs by 2 days (Fig. 1A). Upon necropsy, the de-

velopment of macroscopic lung lesions in infected animals coincided with, and was reciprocal to, weight loss (Fig. 1C). Up to 100% of the lungs were affected by day 3 and 5 p.i. with HeV and NiV, respectively. Lung wet weights were taken as an indicator of inflammation and edema. A >2-fold increase in lung weight could be observed with both HeV- and NiV-infected animals (Fig. 1E). Coinciding with weight loss and lung lesions, HeV infection resulted in a faster increase in lung weight compared to NiV infection.

A low-dose (10^2 $TCID_{50}$) i.n. challenge of NiV or HeV resulted in a more variable outcome of disease compared to the high-dose challenges. HeV challenge resulted in weight loss on days 6 and 7 p.i. (Fig. 1B). By day 7 all HeV-infected animals had to be euthanized due to the development of severe acute respiratory distress as well as the development of neurological signs as described above. Animals infected with NiV did not lose weight but did develop neurological signs as early as 9 days p.i. (Fig. 1B). By day 12 all remaining animals were euthanized due to the development of severe neurological signs. No overt respiratory signs were noticed in these animals.

Lung lesions were detected in HeV-infected animals by day 5 p.i. and covered as much as 100% of the lungs in some animals (Fig. 1D). Lung lesions were also observed in NiV-infected animals on day 9 (Fig. 1D). Interestingly, in NiV-infected animals, lung lesions were clearing on day 10 with only minimal lesions in a few infected animals by days 11 and 12. In accordance with the development of lung lesions, the lung weight of HeV-infected hamsters started to increase by day 5 p.i. and was increased 2-fold by day 6 (Fig. 1F). In NiV-infected animals, the lung weight was increased only on day 9 p.i., in agreement with the transient development of lung lesions in these animals (Fig. 1F).

Radiological changes in NiV- and HeV-infected hamsters. Respiratory disease development was also analyzed by radiographic imaging (X ray). Thoracic radiographic evaluation of both high-dose NiV- and HeV-infected animals was characterized by radiographic changes as early as day 2 p.i. (Fig. 2A and B). Moderate interstitial infiltrates and areas of consolidation were evident in both groups by day 2. Both groups were characterized by rapidly progressive increases of pulmonary infiltrates throughout the lung fields and the formation of air bronchograms. These changes were seen to peak at day 3 p.i. for the HeV-infected animals and at day 5 p.i. for the NiV-infected animals (Fig. 2A and B). Thoracic radiographic changes in animals infected i.n. with a low dose of NiV included diffuse pulmonary interstitial infiltrates first noted on day 5 p.i. (Fig. 2C). Peak radiographic changes were noted on day 9 p.i., with air bronchograms and diffuse pulmonary interstitial infiltrates resulting in complete effacement of the cardiac silhouette. There was a gradual resolution of pulmonary infiltrates on days, 10, 11, and 12. The earliest detectable radiographic changes in animals infected with a low dose of HeV showed focal areas of patchy consolidation in the caudal lung lobes by day 3 p.i. (Fig. 2D). Radiographic lesions were progressively more significant on days 5, 6, and 7. Peak lesions were noted on day 7 p.i. and showed complete effacement of the cardiac silhouette by diffuse pulmonary interstitial infiltrates and detectable air bronchograms.

Virus replication and tissue tropism. A high-dose NiV challenge resulted in efficient virus replication primarily in the respiratory tract (Fig. 3A) with peak titers of 10^6 $TCID_{50}$/gram of tissue in trachea and lungs in all animals. Virus replication in the spleen was observed in 1 animal on day 2 p.i., whereas 1 animal had infectious virus in the brain on day 5 p.i. HeV replication in animals infected with a high dose was found primarily in the respiratory tract (Fig. 3B) with peak titers of 10^6 $TCID_{50}$/gram of lung tissue. In the trachea, infectious virus was found only on days 2 and 3 p.i. In contrast to respiratory tract tropism of NiV infection, low levels of HeV replication were detected in a variety of organs, including spleen, kidney, heart, and brain tissue, suggesting a more systemic spread of the virus (Fig. 3B). Interestingly, no infectious virus could be detected in the blood of either NiV- or HeV-infected animals (data not shown).

Virus replication in the lungs of hamsters infected with a low dose of NiV was 2 logs lower than those infected with a high dose (Fig. 3C). Infectious virus could be detected in the lungs from days 3 to 7 p.i. Interestingly, NiV could be detected in brain tissue as early as day 7 p.i., with peak titers of 10^6 $TCID_{50}$/gram of brain tissue on day 9 p.i. In addition to the lungs and brain, NiV could also be detected in the kidney. A low-dose HeV challenge resulted in systemic spread of the virus to the majority of tissues tested (Fig. 3D). HeV was isolated from the lung early during infection on days 1 and 3 p.i. but by day 5 was spread to all other tissues, including the brain. The highest titers of HeV were found in the brain on day 7 p.i., peaking at 10^7 $TCID_{50}$/gram of brain tissue. Again, no infectious virus was detected in the blood of either NiV- or HeV-infected animals (data not shown).

Cell tropism of NiV and HeV. Infection with both HeV and NiV at a high dose caused primarily pulmonary and upper respiratory lesions (Fig. 4 and Table 1). Lesions were similar between groups but more severe and occurred at earlier time points in HeV-infected animals than in NiV-infected animals (Table 1). Animals in both groups developed necrosuppurative rhinitis (Fig. 4) characterized by variably degenerate nasal epithelium and a mixed submucosal inflammatory infiltrate composed of mononuclear cells admixed with numerous neutrophils. In both groups, infection began as bronchial or peribronchial inflammation, rapidly spreading to the interstitium and ultimately involving pulmonary vessels (data not shown and Fig. 4). Lesions at days 1 and 2 p.i. were characterized by peribronchial neutrophilic and histiocytic infiltrates, small multifocal areas of consolidation, and the rare involvement of small blood vessels, which was especially prominent in HeV-infected animals (data not shown). Viral syncytial cells were often seen in bronchial epithelium and multifocally in areas of inflammation, and these sometimes contained intracytoplasmic eosinophilic viral inclusions (data not shown).

During the late stage of disease (days 3 and 5 for HeV and NiV, respectively), there were widespread areas of necrohemorrhagic bronchopneumonia in both NiV- and HeV-infected animals (Fig. 4), with HeV-infected animals also showing severe perivascular hemorrhage. The bronchial epithelium was variably necrotic in both groups and rarely included epithelial syncytial cells (Fig. 4). There was peribronchial, interstitial, and perivascular hemorrhages, especially severe in HeV-infected animals (Fig. 4). Alveolar lumina were obstructed by a predominantly mononuclear inflammatory cell infiltrate with occasional large viral syncytial cells containing small eosiniphi-

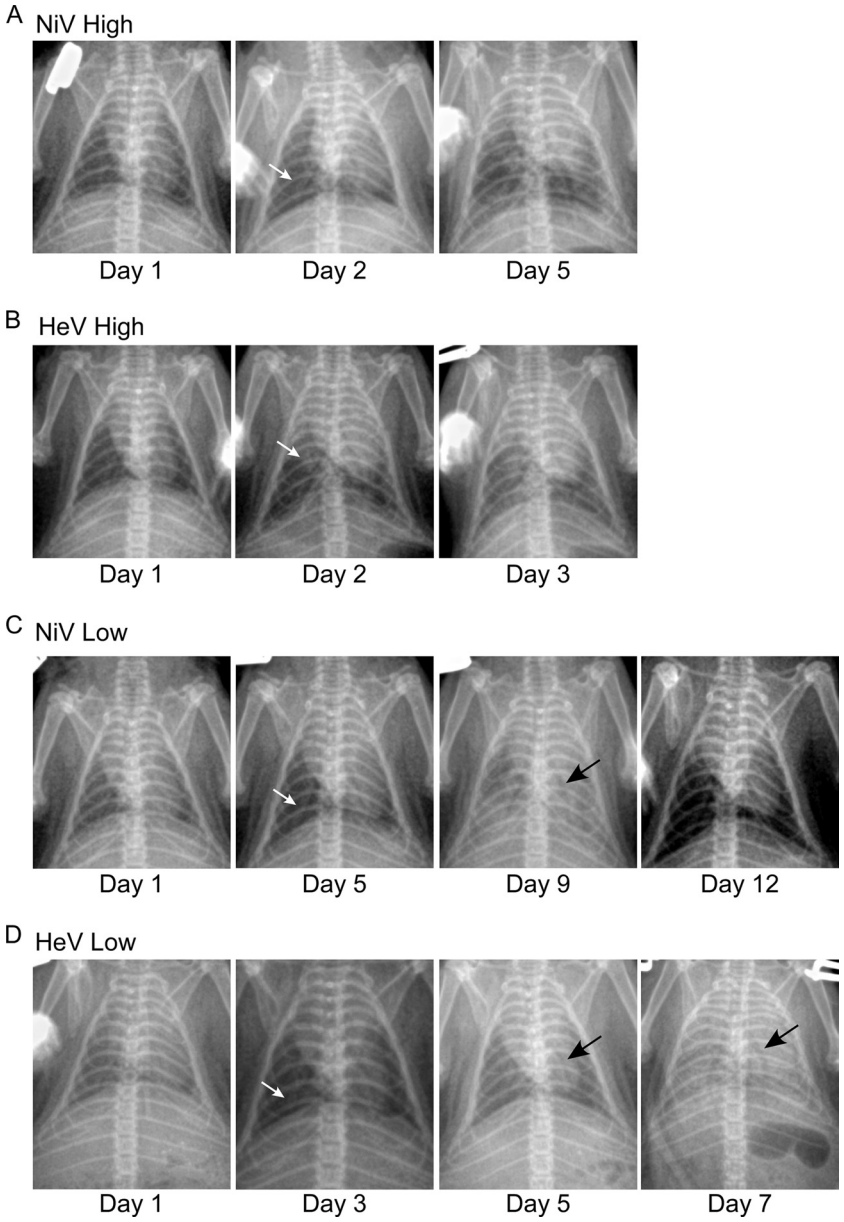

FIG. 2. Radiological examination of the lungs of NiV- and HeV-infected hamsters. Hamsters were infected with a high (A and B) or low (C and D) dose of NiV (A and C) or HeV (B and D). Radiographic images (X-ray) were taken from each group ($n = 5$) prior to euthanasia. Shown are X-rays of a representative animal from each group. White arrows represent earliest detectable radiographic changes. Black arrows represent discernible air bronchograms.

lic intracytoplasmic inclusion bodies (Fig. 4). Again, hemorrhage was a striking feature in HeV-infected animals (Fig. 4). Vascular involvement with endothelial syncytial cell formation and transmural necrotizing vasculitis became more prominent at day 2 p.i. in HeV-infected animals and at days 3 and 4 p.i. in NiV-infected animals (date not shown). This was a major feature by day 3 p.i. in HeV-infected animals and day 5 p.i. in NiV-infected animals (Fig. 4). Alveolar hemorrhage, edema, and fibrin exudation increased as the severity of vascular lesions increased and were more severe in HeV-infected animals than in NiV-infected animals.

Viral nucleocapsid protein (NP) expression in lungs of hamsters infected with a high dose of NiV or HeV generally coincided with an increasing severity of histopathological changes (Fig. 5 and Table 1). The nasal mucosa stained positive in both groups (data not shown), and interestingly, viral NP was detected only in the tracheal epithelium of NiV-infected animals early during infection (Fig. 5 and Table 1). In the NiV-infected animals, viral antigen was noted in the trachea, bronchi, and interstitium from days 1 to 3 p.i. and spread to the vessels at days 4 and 5 p.i., as tracheal staining was absent and bronchial staining intensity waned (Table 1). In HeV-infected animals, no viral antigen was detected in the tracheal epithelium at any time point (Fig. 5 and Table 1). Viral antigen was most abun-

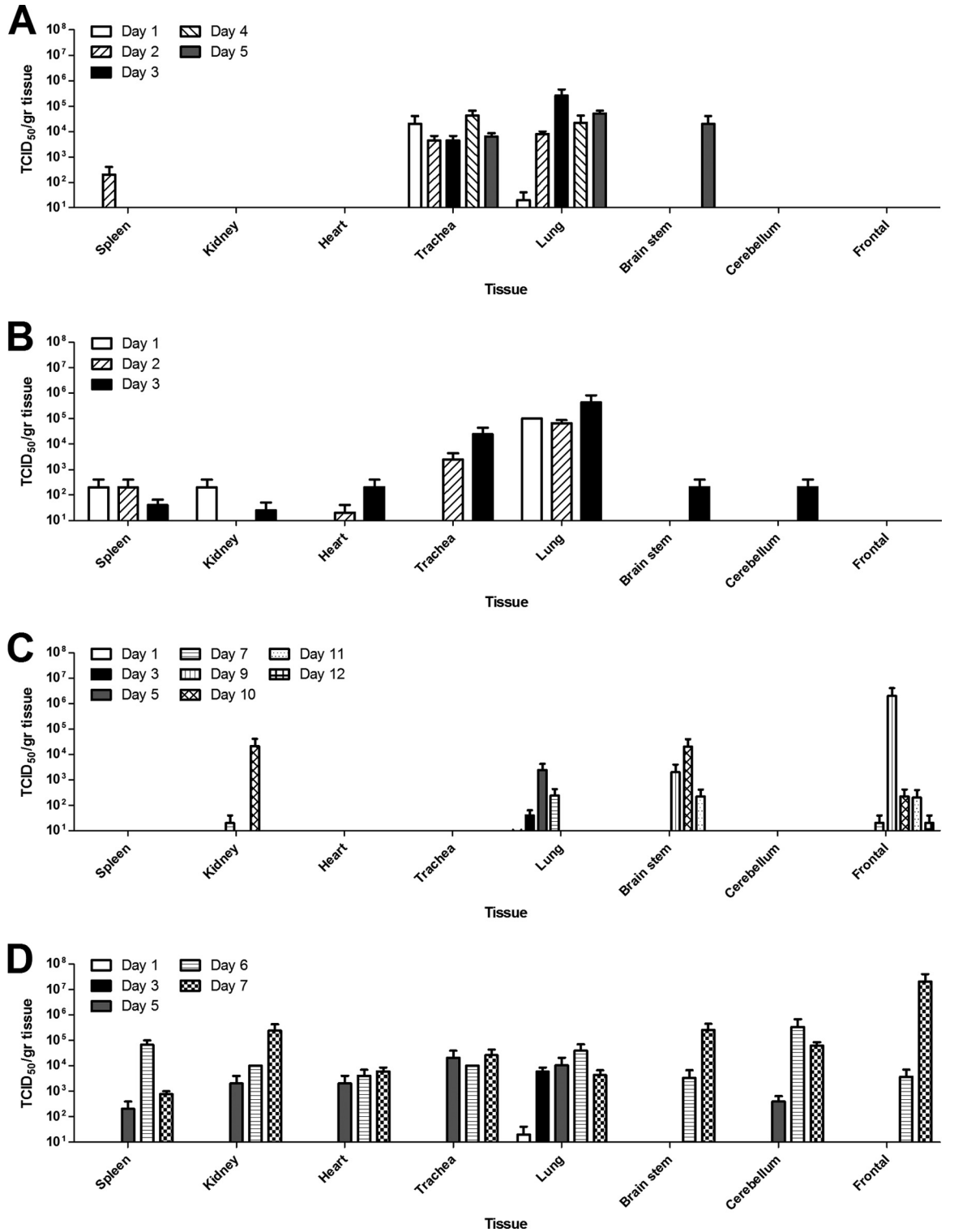

FIG. 3. Virus replication in NiV- and HeV-infected hamsters. Organs were harvested from hamsters infected with a high (A and B) or low (C and D) dose of NiV (A and C) or HeV (B and D) on various days postinfection as described in Materials and Methods. Tissue samples from 5 animals per group were analyzed at each time point. Error bars represent standard deviations.

dant in multifocal peribronchial areas in the interstitium early during infection which became more prevalent by days 2 and 3 p.i. (Fig. 5). HeV spread to the vessels at day 2 p.i. and, unlike NiV, was uncommon in the bronchial epithelium at all time points (Fig. 5 and Table 1). Pulmonary vessels showed the presence of viral antigen in both endothelial cells and transmurally through vascular smooth muscle. No viral antigen was observed in the brains of any animals (Table 1).

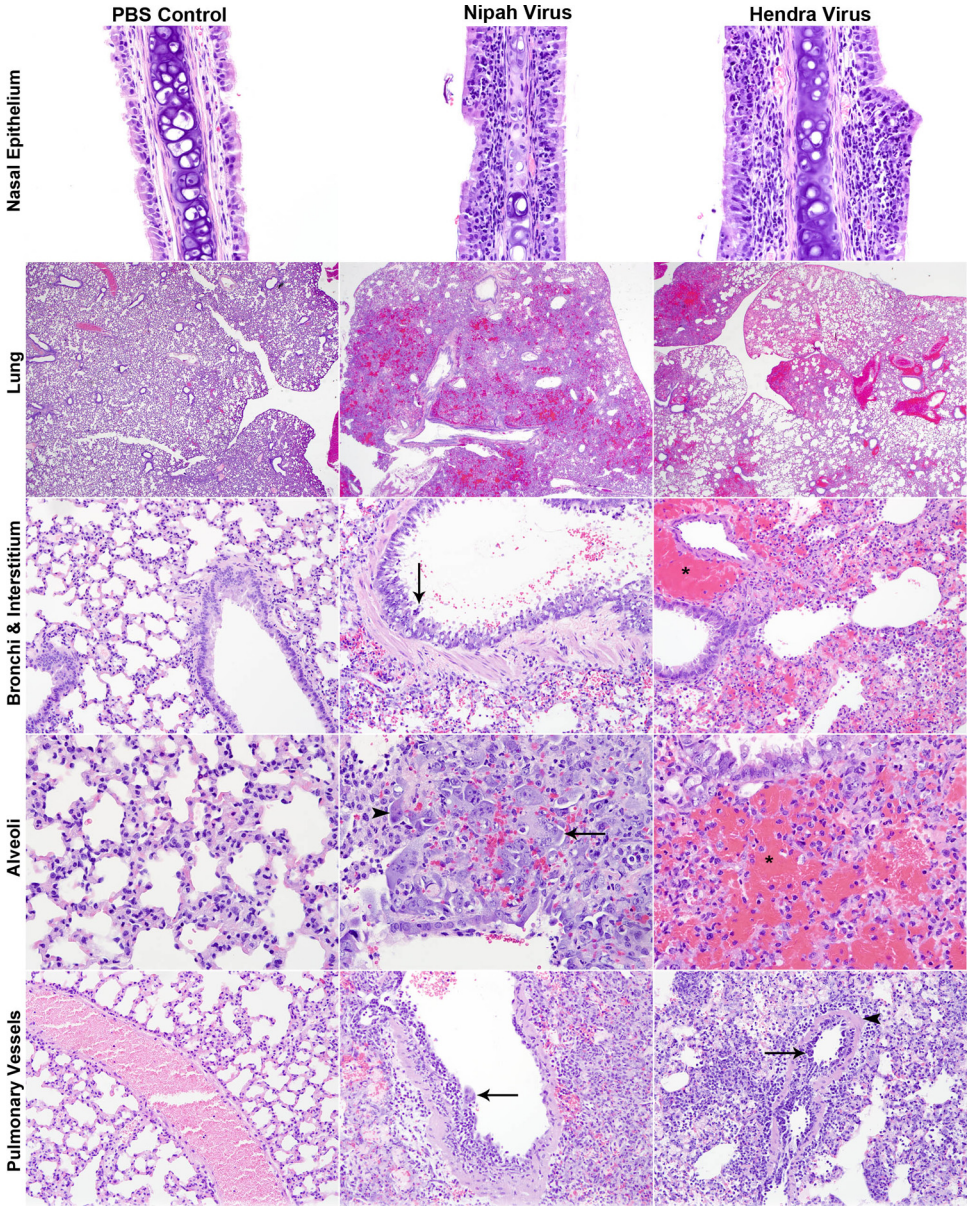

FIG. 4. Histopathological comparison of high-dose NiV- and HeV-infected animals to control animals (PBS). Lung sections were stained with H&E as described in Materials and Methods, and light photographs of the nasal epithelium, lung, bronchi, interstitium, alveoli, and pulmonary vessels of 6-week-old hamsters inoculated with PBS, NiV, or HeV are shown. Nasal epithelium: day 2 p.i.; magnification, ×40. Lung: days 5 and 3 p.i. for NiV and HeV, respectively; magnification, ×2. Bronchi and interstitium: days 5 and 3 p.i. for NiV and HeV, respectively; magnification, ×20. Arrow, epithelial syncytial cells; asterisk, perivascular hemorrhage. Aveoli: days 5 and 3 p.i. for NiV and HeV, respectively; magnification, ×40. Arrow, syncytial cells; arrowhead, eosinophilic intracytoplasmic inclusion bodies; asterisk, hemorrhage. Pulmonary vessels: days 5 and 3 p.i. for NiV and HeV, respectively; magnification, ×20. Arrow, endothelial syncytial formation; arrowhead, transmural necrotizing vasculitis.

In contrast to the high-dose infections, low-dose infections with both HeV and NiV caused lesions in all organs examined, including heart, liver, kidneys, bladder, brain, lungs, and nasal epithelium (data not shown). Pulmonary lesions in the low-dose groups were similar to those in the high-dose groups but had a more protracted course (Table 1). As with the high-dose infections, HeV-infected animals had a more rapid onset of pathological changes, and these changes tended to be more severe compared to those for NiV.

Involvement of nonrespiratory organs began by day 5 p.i. in HeV-infected animals and on day 9 p.i. in NiV-infected animals and continued through the completion of the study (data not shown). Consistent with vascular spread, changes were generally noted in multiple organs of the same animal and were characterized by multifocal neutrophilic, histiocytic, and lymphocytic inflammation with or without necrotizing vasculitis (data not shown). Brain lesions were characterized by moderate or severe lymphohistiocytic meningitis with or without vasculitis (Fig. 6), with multifocal areas of neuropil vacuolation, hemorrhage, neuronal necrosis, and gliosis. Lesions were

TABLE 1. Severity of histopathological changes in lung and virus tropism in lung and brain of Hendra virus- and Nipah virus-infected hamsters[a]

Dose	Virus	Day postinfection	Lung score	Immunohistochemistry				
				Tracheal epithelium	Bronchi	Pulmonary vessels	Interstitium	Brain
High (10^5 $TCID_{50}$)	Hendra	1	+	−	−	−	++	−
		2	++	−	−	+	+++	−
		3	++	−	−/+	+	+++	−
	Nipah	1	+	−/+	−	−	+	−
		2	+	++	+	−	+	−
		3	++	++	++	−/+	++	−
		4	++	−/+	++	−/+	++	−
		5	+++	−	+	++	+++	−
Low (10^2 $TCID_{50}$)	Hendra	1	+	−	−	−	−/+	−
		3	+	−	−	−	+	−
		5	++	−	−/+	+	+++	−/+
		6	+++	−	−	++	+++	+
		7	+++	−	−	+	+++	+++
	Nipah	5	+	−	−	−	−	−
		7	++	−	−	−/+	+	−
		9	++	−	−	+	+	−/+
		10	++	−	−	+	+	++
		11	+	−	−	−	−	++
		12	+	−	−	−	−	+

[a] Lung score and immunohistochemistry: −, absence of lesions; +, inflammation affecting <10% of tissue; ++, inflammation affecting 10 to 50% of tissue; +++, inflammation affecting >50% of tissue; −/+, inflammation in some but not all animals.

randomly distributed throughout the brain, affecting the cerebrum, cerebellum, hippocampus, and olfactory cortex simultaneously.

Immunohistochemical staining for NiV and HeV NP in tissues of hamsters infected with a low dose showed strong antigen positivity in the lungs and brain of both HeV- and NiV-infected animals (Table 1). In the lungs, immunohistochemical (IHC) staining was most intense in the interstitium and pulmonary vessels, with rare staining in bronchi (Table 1). Brains stained positive for viral antigen beginning at day 5 p.i. in HeV-infected animals and day 9 p.i. in NiV-infected animals (Fig. 6 and Table 1). Blood vessels (Fig. 7A), neurons (Fig. 7B), glial cells (Fig. 7C), neuropil (Fig. 6), ependyma, and meninges (Fig. 6) all stained positive for viral antigen, consistent with vascular spread. In the HeV-infected animals, the endothelium of small cerebral blood vessels stained positive before other cells in the brain (Fig. 7A), lending further support for the vascular spread of the virus. No staining in the cranial nerves of any animal was observed, though small blood vessels adjacent to facial nerve bundles were rarely immunoreactive (data not shown).

BBB permeability. The effect of NiV and HeV infection on the permeability of the BBB was determined with hamsters inoculated with NiV and HeV by staining with Evans blue. With an intact BBB, Evans blue will not penetrate the brain; however, as the BBB breaks down, Evans blue is allowed into the central nervous system (CNS). A breakdown of the blood-brain barrier occurred only in animals that displayed neurological signs, as demonstrated by the presence of Evans blue in the brains of these animals (Fig. 8). No sign of positive staining of the brain was shown in any of the control hamsters inoculated with PBS. In contrast, deep-blue-stained lesions were visible on both the dorsal and ventral surfaces of the brains of NiV-infected animals showing severe neurological signs, including partial or complete paralysis of the hind legs. In HeV-infected animals there was light-blue staining of both the dorsal and ventral surfaces of the brain in animals with mild neurological signs.

Host gene expression in lungs and brain of NiV- and HeV-infected hamsters. In order to elucidate the molecular mechanisms of HeV and NiV pathogenesis, the host gene expression of several cytokines and chemokines was determined in lung and brain tissues of infected versus uninfected hamsters. A high dose of either NiV or HeV challenge resulted in the upregulation of IP-10 and several cytokines, including IL-6, IL-4, and IFN-γ in the lung (Fig. 9A, B, C, and D). While IP-10 upregulation was detected as early as day 1 p.i. in HeV-infected lungs, peak expression levels for this chemokine, IL-6, IL-4, and IFN-γ were observed later in the disease on days 2 and 3 and day 5 p.i. for HeV- and NiV-infected animals, respectively. Induction of IP-10 resulted in an up-to-178-fold increase. TNF-α expression was upregulated only early during NiV and HeV infection in the lungs (Fig. 9G).

Interestingly a low-dose infection of NiV and HeV resulted in early downregulation of many of the chemokines and cytokines in the brain (Fig. 9). In agreement with observations of upregulation in the lungs of animals infected with NiV and HeV, IP-10 was also highly upregulated in the brain with peak changes 240-fold for HeV and 37-fold for NiV-infected animals (Fig. 9A). However, upregulation of gene expression was delayed compared to that in the lungs of animals infected with a high dose. In fact, downregulation was observed during the early stages of HeV and NiV infection (first 3 or 5 days, respectively). Expression of IL-6, IL-4, IFN-γ, IL-10, and IL-1β was downregulated in the brain during the early stages of NiV infection, with upregulation apparent only by day 10 p.i.

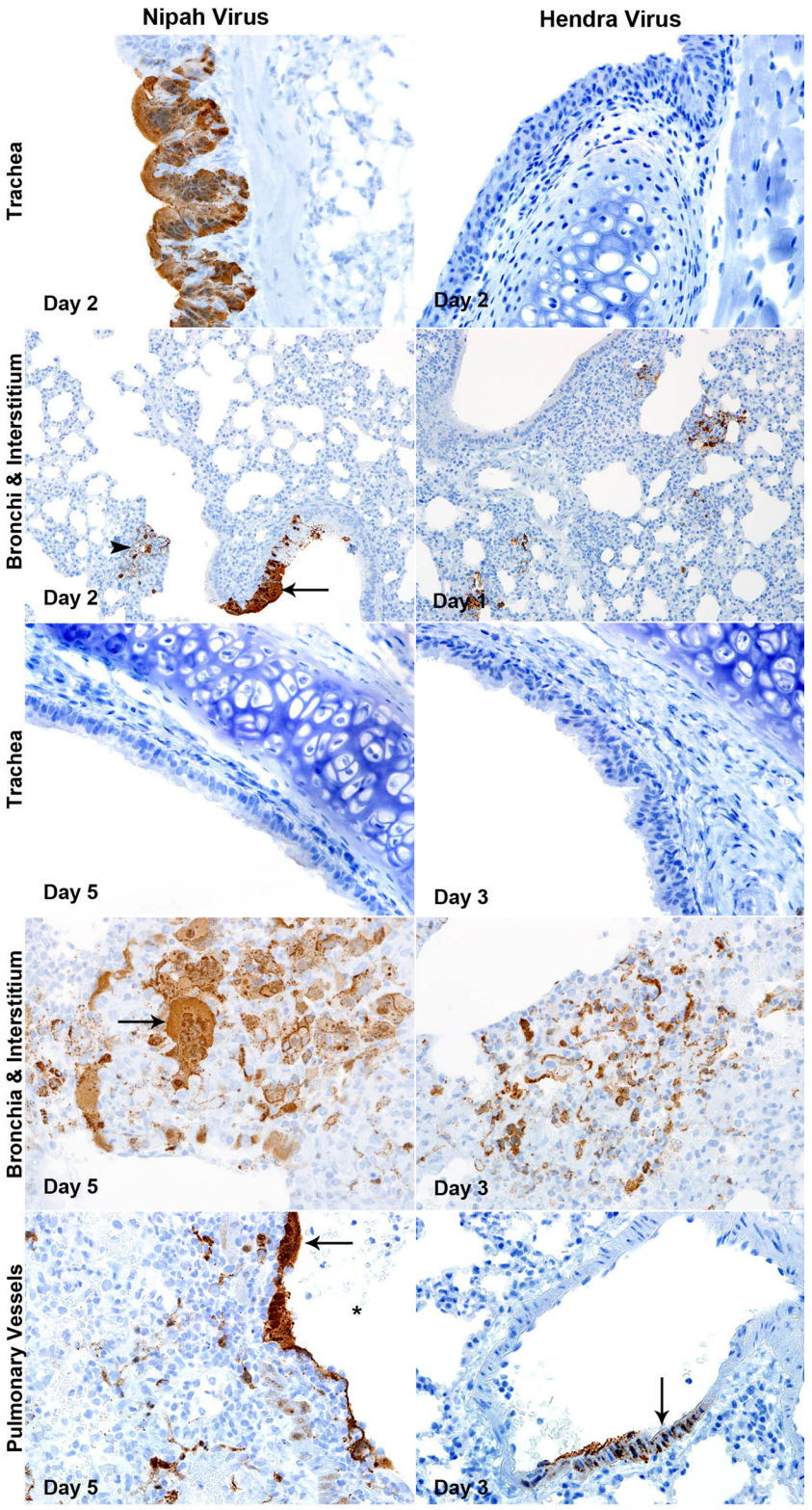

FIG. 5. Tropism of lethal Nipah virus (NiV) and Hendra virus (HeV) in trachea, bronchi, interstitium, and pulmonary vessels of hamster infected with a high dose at various days postinfection. Lung sections were stained for NiV and HeV nucleoprotein as described in Materials and Methods. Trachea: NiV days 2 and 5 p.i., HeV days 2 and 3 p.i.; magnification, ×40. Bronchi and interstitium: NiV days 2 and 5 p.i. (magnification, ×20 and ×40, respectively), HeV days 1 and 3 p.i. (magnification, ×20 and ×40, respectively). Arrow, syncytial cells; arrowhead, cells in interstitium. Pulmonary vessels: day 5 and 3 for NiV and HeV, respectively; magnification, ×40. Arrow, vascular endothelial cells and smooth muscle.

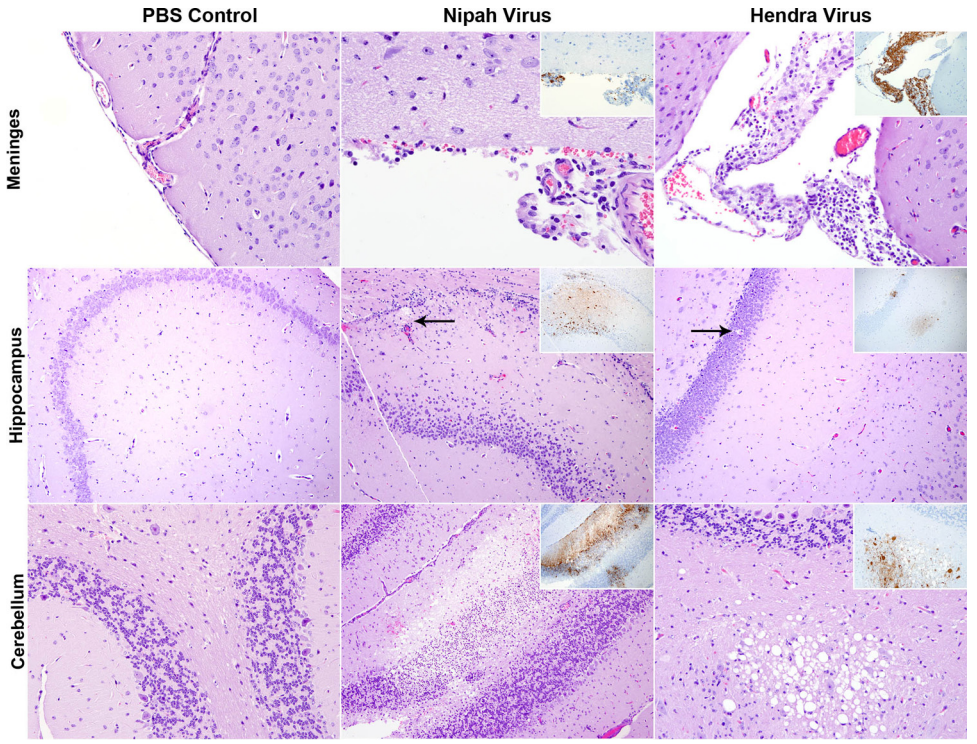

FIG. 6. Brain lesions in animals infected with a low dose of Nipah virus (NiV) and Hendra virus (HeV) compared with those in PBS control animals. NiV- and HeV-infected hamsters were euthanized on days 10 and 7 p.i., respectively, and lung sections were stained with H&E and stained for NiV and HeV nucleoprotein (NP; insets) as described in Materials and Methods. Light photographs of the meninges, hippocampus, and cerebellum of 6-week-old hamsters inoculated with PBS, NiV, or HeV are shown. Meninges: magnification, ×20. Hippocampus: magnification, ×10. Arrow for NiV, areas of hemorrhage and malacia; arrow for HeV, single cell neuronal necrosis. Cerebellum: NiV, magnification, ×10; HeV, magnification, ×20.

(Fig. 9B to F). These cytokine genes were also upregulated during the final stage of HeV infection in the brain, and only IFN-γ, IL-10, and IL-1β expression was downregulated during the first 3 to 5 days p.i. (Fig. 9D to F). TNF-α expression peaked at 1 to 2 days prior to the moribund stage of both HeV and NiV infection (Fig. 9G). Interestingly, while chemokine and cytokine expression generally peaked during the final stage of high-dose NiV and HeV infection in the lung as well as low-dose HeV infection in the brain, peak expression in the brains of animals infected with a low dose of NiV was observed generally 2 days prior to the moribund stage of disease.

DISCUSSION

Hendra and Nipah viruses are newly emerging zoonotic viruses that can cause severe respiratory illness and encephalitis in humans (18). Despite intensive studies, little is known about the mechanisms governing the development of respiratory and/or neurological disease. The goal of the present study was to characterize the respiratory and neurological disease manifestations in the hamster model and to study the role of the host response in HeV and NiV pathogenesis.

While several animals models have been described for both

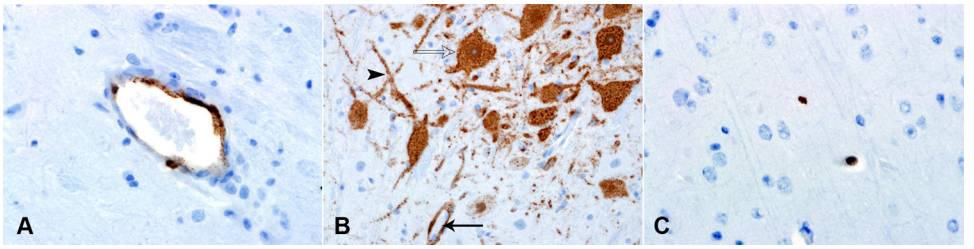

FIG. 7. Blood vessels, neurons, and glial cells are immunoreactive in animals infected with low-dose HeV and NiV. Brain sections were stained for NiV and HeV NP as described in Materials and Methods. (A) Viral NP expression in endothelial cells of small blood vessels throughout the cerebellum of HeV-infected hamsters on day 6 p.i. Magnification, ×100. (B) Viral NP expression in neurons of HeV-infected hamsters on day 7 p.i., including both cell bodies (open arrow) and dendrites (arrowhead), as well as endothelial cells of small blood vessels (closed arrow), magnification, ×40. (C) Viral NP expression in glial cells of HeV-infected hamsters on day 6 p.i., magnification, ×100.

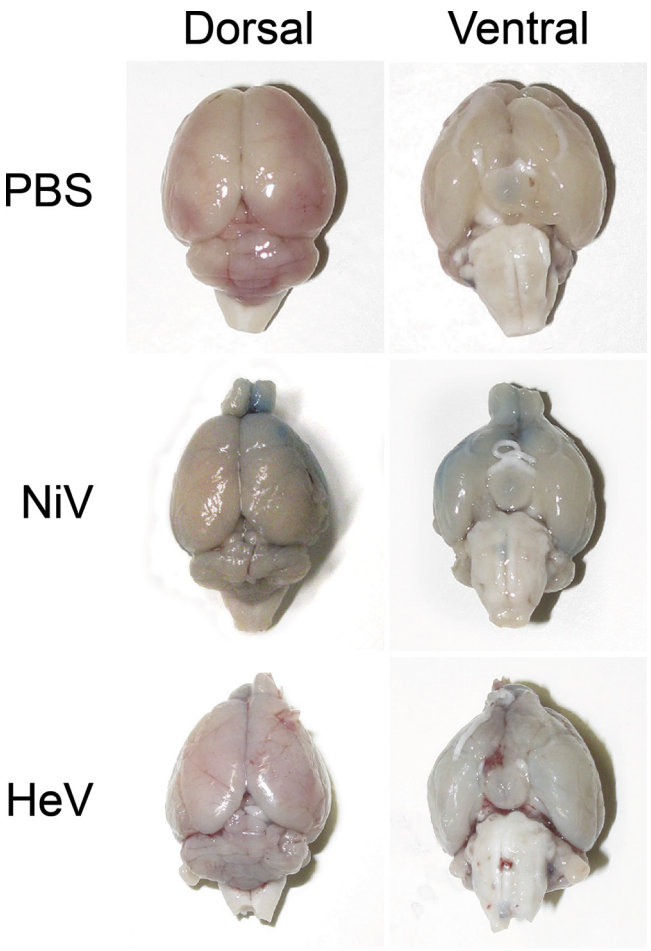

FIG. 8. Blood-brain barrier permeability is associated with neurological disease following NiV and HeV infection. Hamsters inoculated with PBS, NiV, or HeV were injected with Evans blue 24 h prior to euthanasia as described in Materials and Methods. Evans blue was detected on the dorsal and ventral sides of the brains of NiV- and HeV-infected animals due to an increase in blood-brain barrier permeability.

HeV and the related NiV, studies on pathogenesis and the development of effective therapeutics have been somewhat limited due to biocontainment restrictions for work with these infectious agents (34). Recently, uniformly lethal nonhuman primate (NHP) models were described for HeV and NiV that recapitulated both the respiratory and neurological components of disease (11, 29). Interestingly, ribavirin treatment of HeV-infected NHP effectively lowered virus titers which apparently precluded the development of respiratory signs (29). The treatment did not seem to prevent systemic spread of the virus, and infection of the central nervous system (CNS) could be established (29). We hypothesized that the infectious dose determines the clinical outcome of NiV and HeV infection.

Hamsters have been shown to recapitulate acute HeV and NiV infections, as seen with humans, developing severe respiratory disease and encephalitis (13, 35), and have been used in several studies to successfully test antiviral therapeutic strategies (12, 13, 26). However, the clinical aspect of these infections and the effect of the challenge route and dose have not been well studied. In the current study a high-dose intranasal challenge with either NiV or HeV resulted in severe acute respiratory distress, with lesions and radiological changes appearing as early as 1 day p.i. While HeV and NiV replicated primarily in the respiratory tract, low-level systemic infection was detected, based on the presence of virus in the periphery following i.n. challenge, in agreement with observations in NHP and human cases (11, 29, 36, 37). NiV infection of the respiratory tract was initiated in the trachea as early as day 1, progressed down the respiratory tract, infecting the bronchial epithelium, and finally caused severe hemorrhagic pneumonia, including the characteristic syncytium formation in the pulmonary endothelium. In contrast, HeV infection was initiated primarily in the interstitium of the lungs and not in the trachea or bronchi. Endothelial cells have previously been identified as an important target of infection; however, this was based on observations from lethal human cases of HeV and NiV and therefore represents only the final stages of the disease (20, 36, 37). Our data clearly show that while endothelial cells are an important target of HeV and NiV infection during the late stages of disease, the respiratory epithelium is the primary target of HeV and NiV infection. The observation that NiV but not HeV can replicate efficiently in the upper respiratory tract may also have implications for the transmissibility of these viruses, with NiV being potentially more transmissible compared to HeV. These differences in initial sites of replication may explain the fact that human-to-human transmission has been observed only during outbreaks of NiV but not HeV infection (2, 10, 14). Initiation of HeV infection would require the virus to reach the lower respiratory tract, making transmission less efficient. This is similar to the observations that efficiently transmitted seasonal and pandemic influenza viruses attach better to the upper respiratory tract epithelium, whereas avian influenza viruses do not (32), as well as to the observation of the adaptation of severe acute respiratory syndrome coronavirus (SARS-CoV) to efficiently replicate in the human upper respiratory tract epithelium (31). Studies of the transmissibility of these viruses are currently ongoing.

A low-dose i.n. challenge of HeV in hamsters resulted in a slower onset of clinical signs, allowing for systemic spread of the virus and ultimately the development of both respiratory and neurological disease. Interestingly, NiV infection resulted in a transient respiratory infection followed by the development of neurological signs. This is similar to observations with humans in which HeV and NiV cases initially present with ILI, which can progress to encephalitic manifestations (18, 36). The observed systemic spread of NiV and HeV to other organs suggests a viremic stage during infection. While we were unable to recover infectious virus from the blood of infected animals, HeV RNA has been detected in this model previously, suggesting the low-level presence of virus (13). HeV and NiV infection of the CNS and the development of neurological signs were associated with the disruption of the BBB. It has been shown previously that Nipah virus can invade the CNS of pigs by crossing the blood-brain barrier after initial virus replication in the upper respiratory tract (33); to our knowledge, this is the first description of BBB disruption by HeV and NiV, and studies are ongoing to determine whether this disruption is the direct or indirect effect of virus infection.

Several cytokines and especially IP-10 were upregulated dur-

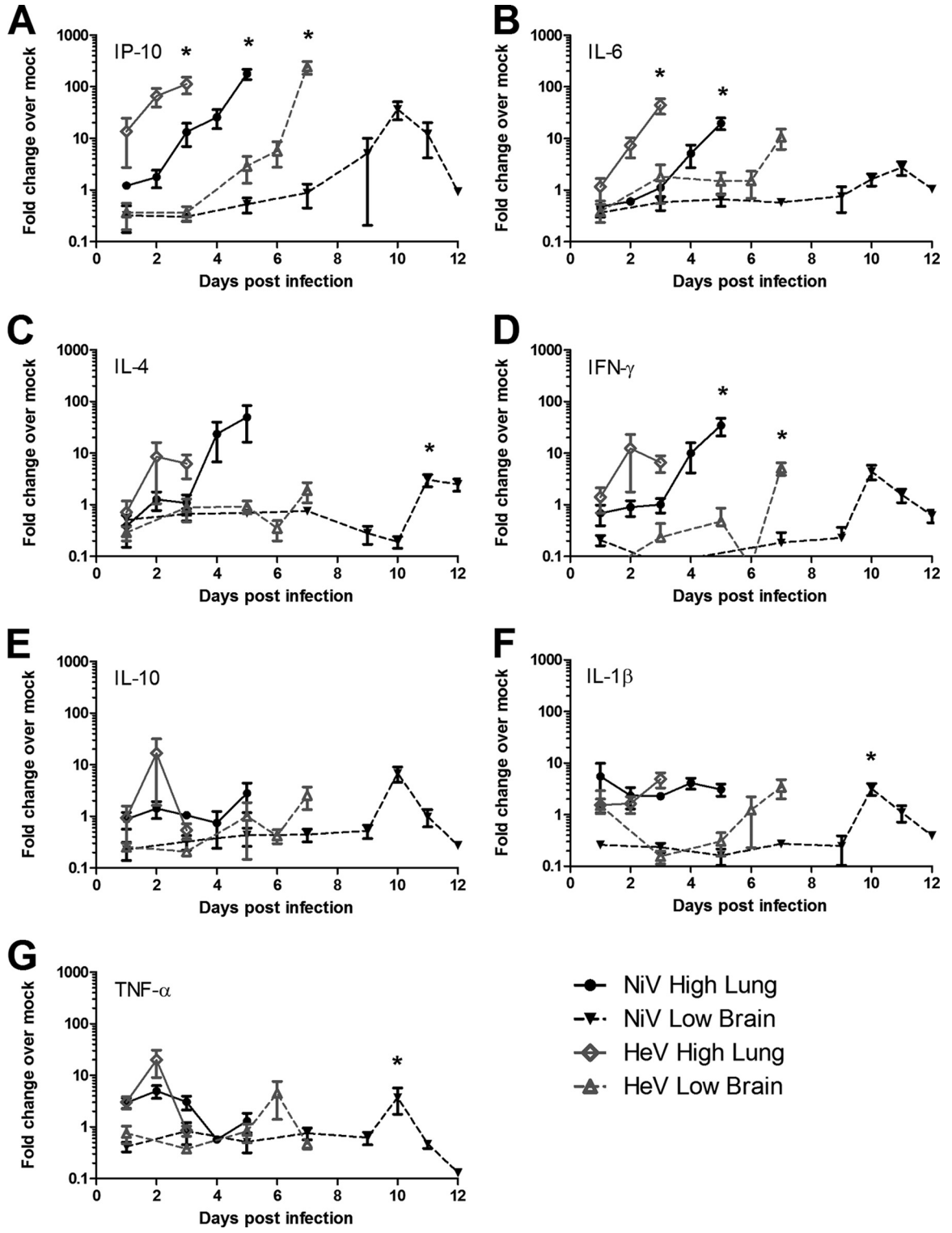

FIG. 9. Host gene expression in the lungs and brains of hamsters following NiV and HeV infection. Quantitative RT-PCR for IL-1β (A), IP-10 (B), IL-4 (C), IFN-γ (D), IL-6 (E), TNF-α (F), and IL-10 (G) was performed on lung samples (● and ◇) from groups of 5 hamsters infected with a high dose of NiV (black) or HeV (gray) and brain samples (▼ and Δ) from hamsters infected with a low dose of NiV (black) or HeV (gray). The data are shown as changes over mock-infected controls. The error bars represent standard deviations. *, significantly different from PBS controls, $P < 0.05$; analysis of variance (ANOVA).

ing henipavirus infection in both respiratory and CNS tissues. Expression of IP-10 was highly upregulated in both lung and brain tissue and was associated with virus replication in these tissues. The upregulation of IP-10 also correlated with the influx of inflammatory cells observed with both these tissues. Upregulation of IP-10, IL-1β, IL-6, TNF-α, and IFN-γ in the lungs has been described to play a role in the pathogenesis of several respiratory virus infections, including SARS-CoV and H5N1 (3, 6, 28). These inflammatory mediators also play an important role in acute respiratory distress syndrome (ARDS) pathophysiology (27). In the brain, the timing of TNF-α and IL-1β upregulation followed the first occurrence of infectious NiV and HeV in the brain. The proinflammatory cytokines TNF-α and IL-1β have been shown to play an important role in the induction of neuronal injury and death as well as increase the permeability of the blood-brain barrier (5). Both cytokines can be released by microglia, which were also shown to be infected by NiV and HeV in this study (5).

In addition to the potential role of TNF-α in the pathogenesis of NiV- and HeV-induced neurological disease, it may also serve as a biomarker for the lethal outcome of NiV and HeV infection, as it was typically upregulated in both lungs and the brain 1 to 2 days prior to death. To our knowledge this is the first characterization of the host responses against HeV and NiV infection.

Previous studies, describing the hamster model of HeV and NiV, focused on a general description of the pathogenesis and the similarities between the two viruses for the establishment of robust challenge models to evaluate vaccine and therapeutic approaches (13, 35). Interestingly, the LD_{50} determined for the i.n. challenge route in this study is >2,000-fold lower than that from a previous study (35). While this difference could be due to possible genetic differences between the NiV challenge stocks, a more likely explanation is the difference in challenge volumes for the i.n. route. The 3-fold-higher volume used in the current study ensures inoculation of the viruses deep into the lungs and establishes a more robust and uniform infection, similar to what was seen with infection with SARS-CoV and influenza virus in mice (unpublished data; 17).

This study clearly shows that differences in the clinical outcome of disease can be achieved by only changing the initial challenge dose. Previous epidemiological studies have shown significant differences in clinical presentations between the initial outbreaks of NiV in Malaysia and the subsequent outbreaks in Bangladesh (18). The Bangladesh strain of NiV was associated with a higher prevalence of respiratory distress (70%) than that of the Malaysia strain (14 to 27%). While these observed differences could be due to genetic differences between the two NiV strains, our data suggest that the transmission route and dose can also affect the clinical outcome. Direct contact with infected pigs was a major risk factor in the Malaysia outbreaks (24), whereas human-to-human and bat-to-human transmission through contaminated food were major risk factors during the Bangladesh outbreaks (14, 22). These differences in transmission can easily affect the infectious dose and result in different clinical presentations. Studies of the clinical outcome of oral infection are under way.

In conclusion, our data show that differences in the infectious dose result in different clinical presentations. We believe that these models allow for more detailed studies of the pathogenesis of respiratory or neurological disease caused by HeV and NiV infection. In addition this study demonstrates that the respiratory epithelium serves as the initial site of HeV and NiV replication, which is followed by systemic spread and ultimately infection of the CNS, and that infection of the CNS results in the disruption of the BBB. These data provide several target cytokines that are associated with lethal NiV and HeV infection and specifically identify IP-10, IL-1β, and TNF-α as important and potential targets for treatment.

ACKNOWLEDGMENTS

We thank Tina Neisinger, Rebecca Rosenke, Lisa Kercher, Rachel LaCasse, Kathleen Meuchel, Sandy Skorupa, and Dan Long of the Rocky Mountain Veterinary Branch (DIR, NIAID, NIH) for assistance in animal care and histology and Anita Mora and Gary Hettrick (DIR, NIAID, NIH) and Steve Schuenke (UTMB) for assistance with graphical work.

This study was financially supported by the Division of Intramural Research (DIR), NIAID, NIH.

We declare no conflict of interest.

REFERENCES

1. **Amal, N. M., et al.** 2000. Risk factors for Nipah virus transmission, Port Dickson, Negeri Sembilan, Malaysia: results from a hospital-based case-control study. Southeast Asian J. Trop. Med. Public Health **31:**301–306.
2. **Barclay, A. J., and D. J. Paton.** 2000. Hendra (equine morbillivirus). Vet. J. **160:**169–176.
3. **Baskin, C. R., et al.** 2009. Early and sustained innate immune response defines pathology and death in nonhuman primates infected by highly pathogenic influenza virus. Proc. Natl. Acad. Sci. U. S. A. **106:**3455–3460.
4. **Bossart, K. N., et al.** 2009. A neutralizing human monoclonal antibody protects against lethal disease in a new ferret model of acute Nipah virus infection. PLoS Pathog. **5:**e1000642.
5. **Brabers, N. A., and H. S. Nottet.** 2006. Role of the pro-inflammatory cytokines TNF-alpha and IL-1beta in HIV-associated dementia. Eur. J. Clin. Invest. **36:**447–458.
6. **Cameron, M. J., J. F. Bermejo-Martin, A. Danesh, M. P. Muller, and D. J. Kelvin.** 2008. Human immunopathogenesis of severe acute respiratory syndrome (SARS). Virus Res. **133:**13–19.
7. **Chadha, M. S., et al.** 2006. Nipah virus-associated encephalitis outbreak, Siliguri, India. Emerg. Infect. Dis. **12:**235–240.
8. **Chew, M. H., et al.** 2000. Risk factors for Nipah virus infection among abattoir workers in Singapore. J. Infect. Dis. **181:**1760–1763.
9. **Chua, K. B., et al.** 1999. Fatal encephalitis due to Nipah virus among pig-farmers in Malaysia. Lancet **354:**1257–1259.
10. **Field, H., et al.** 2010. Hendra virus outbreak with novel clinical features, Australia. Emerg. Infect. Dis. **16:**338–340.
11. **Geisbert, T. W., et al.** 2010. Development of an acute and highly pathogenic nonhuman primate model of Nipah virus infection. PLoS One **5:**e10690.
12. **Guillaume, V., et al.** 2004. Nipah virus: vaccination and passive protection studies in a hamster model. J. Virol. **78:**834–840.
13. **Guillaume, V., et al.** 2009. Acute Hendra virus infection: analysis of the pathogenesis and passive antibody protection in the hamster model. Virology **387:**459–465.
14. **Gurley, E. S., et al.** 2007. Person-to-person transmission of Nipah virus in a Bangladeshi community. Emerg. Infect. Dis. **13:**1031–1037.
15. **Homaira, N., et al.** 2010. Nipah virus outbreak with person-to-person transmission in a district of Bangladesh, 2007. Epidemiol. Infect. **138:**1630–1636.
16. **Hsu, V. P., et al.** 2004. Nipah virus encephalitis reemergence, Bangladesh. Emerg. Infect. Dis. **10:**2082–2087.
17. **Iwasaki, T., et al.** 1999. Exacerbation of influenzavirus pneumonia by intranasal administration of surfactant in a mouse model. Arch. Virol. **144:**675–685.
18. **Lo, M. K., and P. A. Rota.** 2008. The emergence of Nipah virus, a highly pathogenic paramyxovirus. J. Clin. Virol. **43:**396–400.
19. **Luby, S. P., E. S. Gurley, and M. J. Hossain.** 2009. Transmission of human infection with Nipah virus. Clin. Infect. Dis. **49:**1743–1748.
20. **Maisner, A., J. Neufeld, and H. Weingartl.** 2009. Organ- and endotheliotropism of Nipah virus infections in vivo and in vitro. Thromb. Haemost. **102:**1014–1023.
21. **McEachern, J. A., et al.** 2008. A recombinant subunit vaccine formulation protects against lethal Nipah virus challenge in cats. Vaccine **26:**3842–3852.
22. **Montgomery, J. M., et al.** 2008. Risk factors for Nipah virus encephalitis in Bangladesh. Emerg. Infect. Dis. **14:**1526–1532.
23. **O'Sullivan, J. D., et al.** 1997. Fatal encephalitis due to novel paramyxovirus transmitted from horses. Lancet **349:**93–95.

24. **Parashar, U. D., et al.** 2000. Case-control study of risk factors for human infection with a new zoonotic paramyxovirus, Nipah virus, during a 1998–1999 outbreak of severe encephalitis in Malaysia. J. Infect. Dis. **181:**1755–1759.
25. **Playford, E. G., et al.** 2010. Human Hendra virus encephalitis associated with equine outbreak, Australia, 2008. Emerg. Infect. Dis. **16:**219–223.
26. **Porotto, M., et al.** 2010. Inhibition of Nipah virus infection in vivo: targeting an early stage of paramyxovirus fusion activation during viral entry. PLoS Pathog. **6:**e1001168.
27. **Puneet, P., S. Moochhala, and M. Bhatia.** 2005. Chemokines in acute respiratory distress syndrome. Am. J. Physiol. Lung Cell Mol. Physiol. **288:**L3–L15.
28. **Rockx, B., et al.** 2009. Early upregulation of acute respiratory distress syndrome-associated cytokines promotes lethal disease in an aged-mouse model of severe acute respiratory syndrome coronavirus infection. J. Virol. **83:**7062–7074.
29. **Rockx, B., et al.** 2010. A novel model of lethal Hendra virus infection in African green monkeys and the effectiveness of ribavirin treatment. J. Virol. **84:**9831–9839.
30. **Selvey, L. A., et al.** 1995. Infection of humans and horses by a newly described morbillivirus. Med. J. Aust. **162:**642–645.
31. **Sheahan, T., B. Rockx, E. Donaldson, D. Corti, and R. Baric.** 2008. Pathways of cross-species transmission of synthetically reconstructed zoonotic severe acute respiratory syndrome coronavirus. J. Virol. **82:**8721–8732.
32. **van Riel, D., et al.** 2010. Seasonal and pandemic human influenza viruses attach better to human upper respiratory tract epithelium than avian influenza viruses. Am. J. Pathol. **176:**1614–1618.
33. **Weingartl, H., et al.** 2005. Invasion of the central nervous system in a porcine host by Nipah virus. J. Virol. **79:**7528–7534.
34. **Weingartl, H. M., Y. Berhane, and M. Czub.** 2009. Animal models of henipavirus infection: a review. Vet. J. **181:**211–220.
35. **Wong, K. T., et al.** 2003. A golden hamster model for human acute Nipah virus infection. Am. J. Pathol. **163:**2127–2137.
36. **Wong, K. T., et al.** 2009. Human Hendra virus infection causes acute and relapsing encephalitis. Neuropathol. Appl. Neurobiol. **35:**296–305.
37. **Wong, K. T., et al.** 2002. Nipah virus infection: pathology and pathogenesis of an emerging paramyxoviral zoonosis. Am. J. Pathol. **161:**2153–2167.
38. **Zivcec, M., D. Safronetz, E. Haddock, H. Feldmann, and H. Ebihara.** Validation of assays to monitor immune responses in the Syrian golden hamster (Mesocricetus auratus). J. Immunol. Methods, in press.